Loss of Axin1 drives acquired resistance to WNT pathway blockade in colorectal cancers cells carrying RSPO3 fusions.

Gabriele Picco[1,2], Consalvo Petti[1,2], Alessia Centonze[2], Erica Torchiaro[1], Giovanni Crisafulli[1], Luca Novara[1], Andrea Acquaviva[3], Alberto Bardelli[1,2] and Enzo Medico*[1,2]

APPENDIX

Table of contents

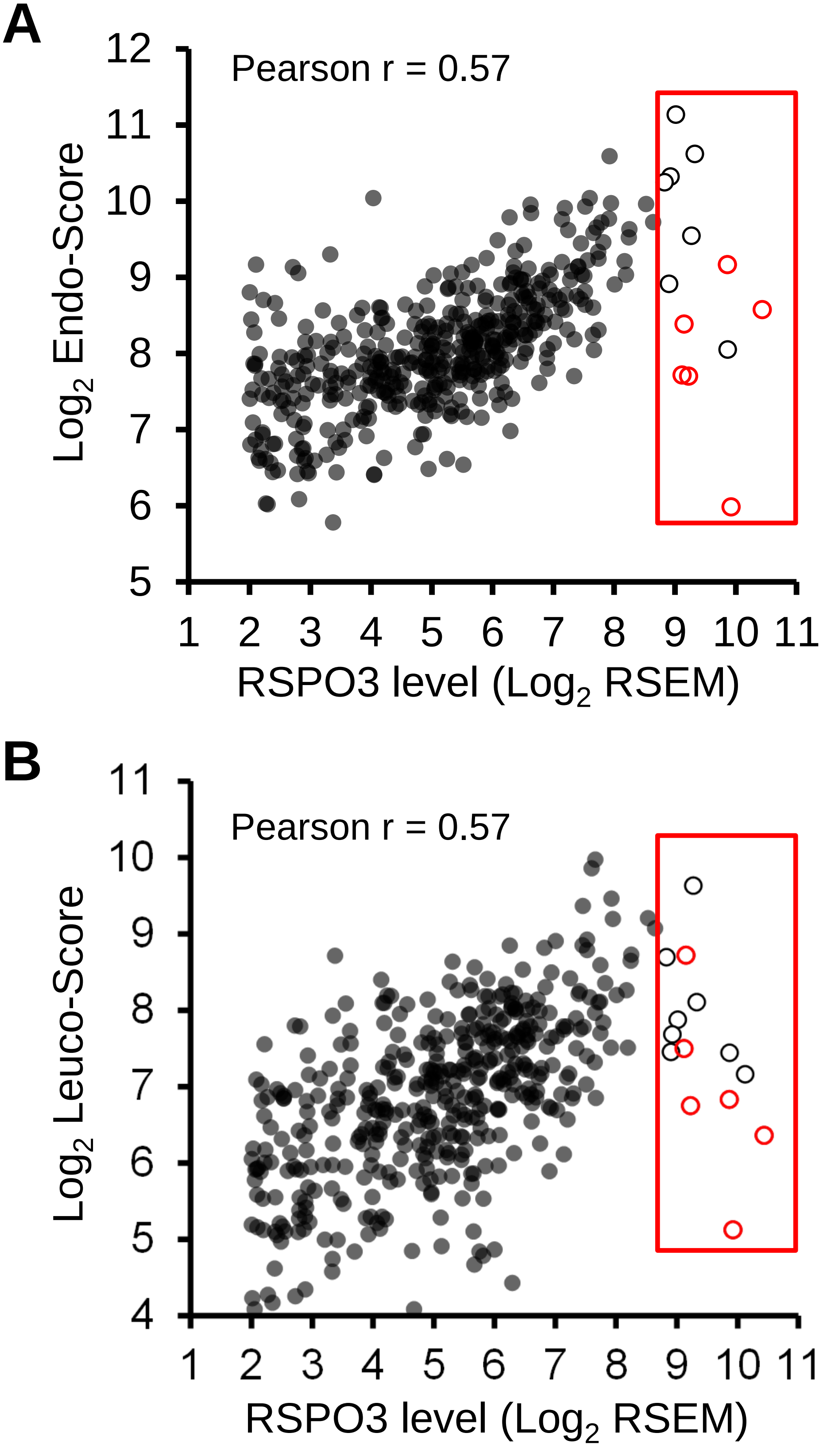

Picco et al., Appendix Figure S1. Stromal scores vs. RSPO3 expression in the TCGA dataset. Scatter plots displaying the correlation between RSPO3 expression levels (x-axis) and Endo-score (A) or Leuco-score (B). The red boxes highlight samples with high RSPO3 expression and variable Endo- or Leuco-score. Empty dots indicate samples selected for fusion analysis. Empty dots with red border indicate samples with high RSPO3 levels and medium-low CAF-score, also highlighted in Figure 1A.

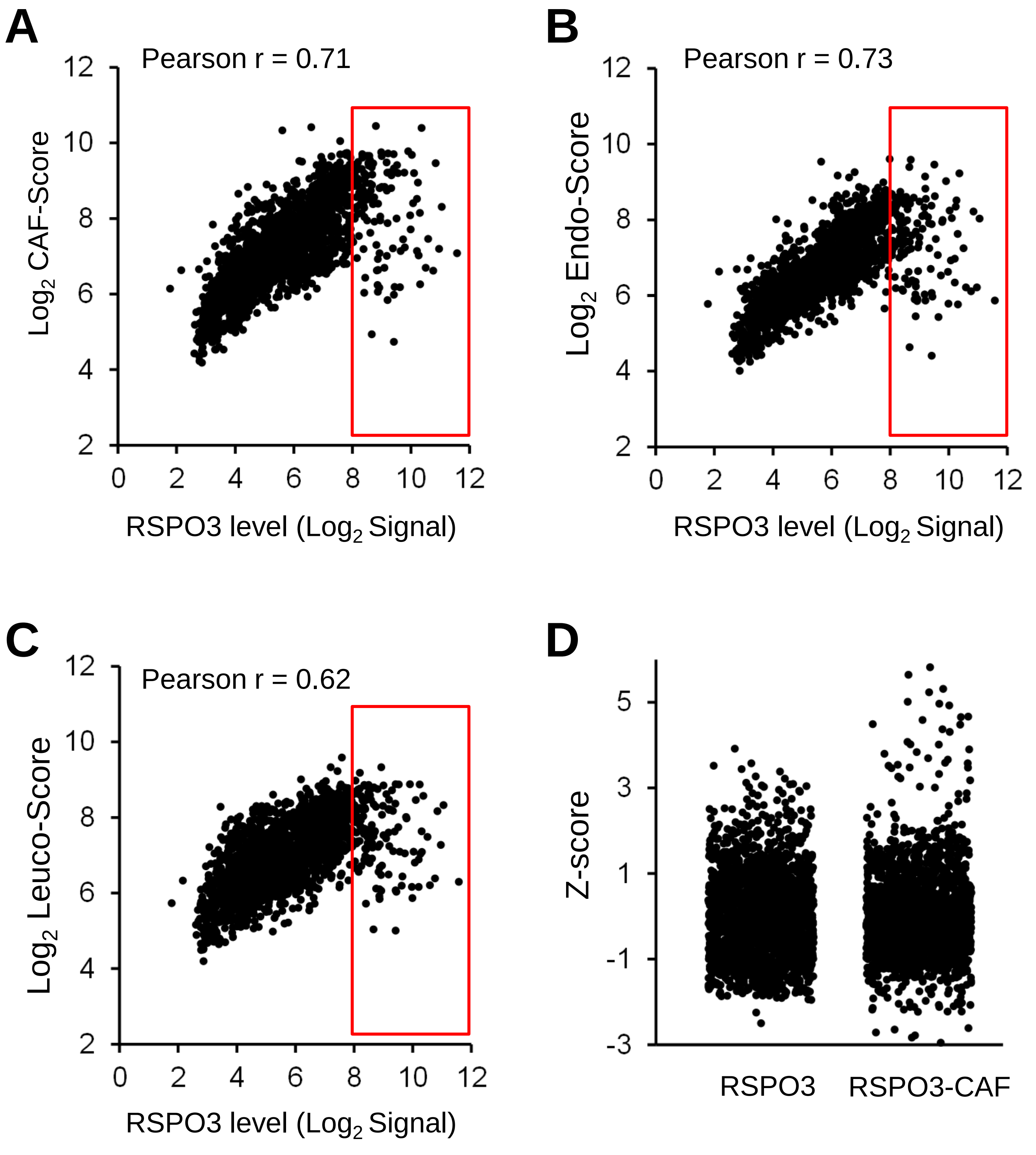

Picco et al., Appendix Figure S2. RSPO3 expression vs. stromal scores in a 2140-sample CRC microarray dataset. A composite CRC gene expression dataset was built from the following public datasets: GSE13294, GSE14333, GSE17536, GSE20916, GSE2109, GSE35896, GSE37892, GSE39582, KFSYSCC. Scatter plots display the correlation between RSPO3 expression levels on the x-axis and CAF-score (A), Endo-score (B) and Leuco-score (C), on the y-axis. The red boxes highlight samples with high RSPO3 expression and variable stromal scores. (D) Dot plots displaying the distribution of Z-Score values for RSPO3 alone and RSPO3 minus CAF-score.

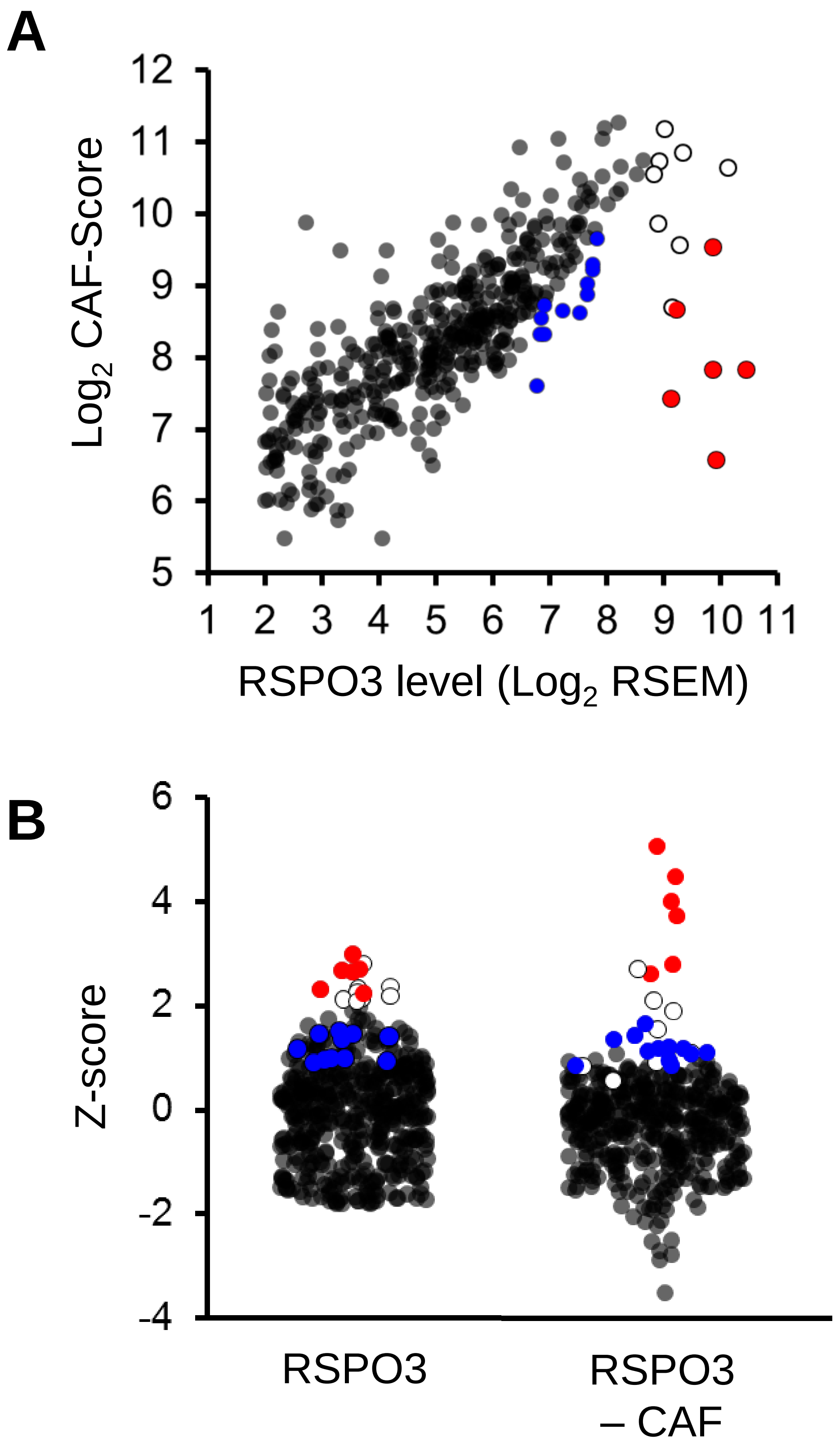

Picco et al., Appendix Figure S3. Absence of RSPO3 rearrangements in 12 additional TCGA CRC samples. (A) Scatter plot displaying the correlation between RSPO3 expression (x-axis) and CAF-score (y-axis). (B) Dot plots displaying the distribution of Z-Score values for RSPO3 alone (left panel) and RSPO3 minus CAF-score (right panel) in the 450-sample TCGA dataset. Blue dots indicate 12 samples with intermediate RSPO3 expression and low CAF-score, selected to complete the search for RSPO3 fusions. Empty dots indicate previously analyzed samples that do not carry RSPO3 fusions. Red dots indicate RSPO3 fused samples.

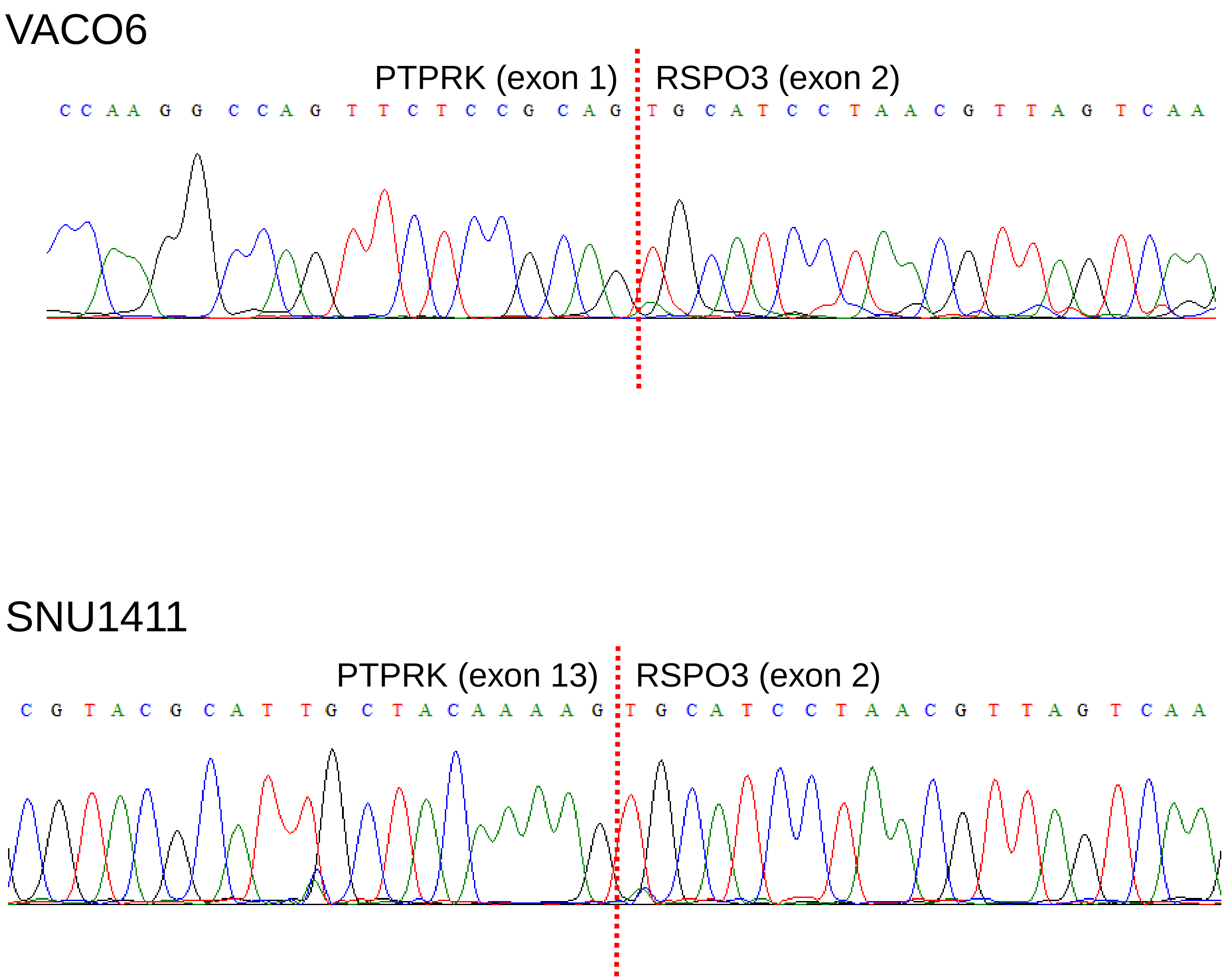

Picco et al., Appendix Figure S4: validation by Sanger sequencing of RSPO3 fusion transcripts in CRC cell lines. Representative Sanger sequencing chromatograms of RT–PCR amplicons confirming the PTPRK(e1)–RSPO3(e2) and the novel PTPRK(e13)–RSPO3(e2) fusion junctions in VACO6 and SNU1411 cells, respectively.

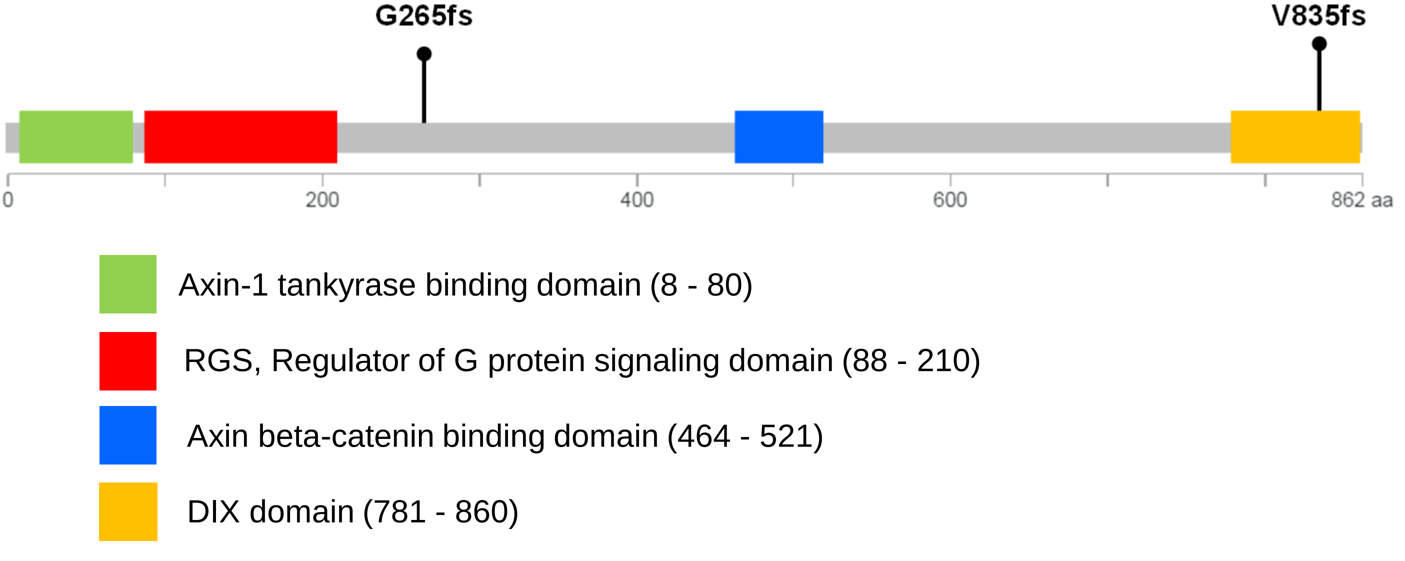

Picco et al., Appendix Figure S5. Axin1 mutations detected in VACO6$_R$. Representation of the two frameshift-inducing single nucleotide deletions in the AXIN1 gene in VACO6$_R$ cells, as reported for human tumor samples by cBioPortal (www.cbioportal.org; Cerami et al., Cancer Discov. 2012). Color-coded rectangles highlight AXIN1 protein domains.

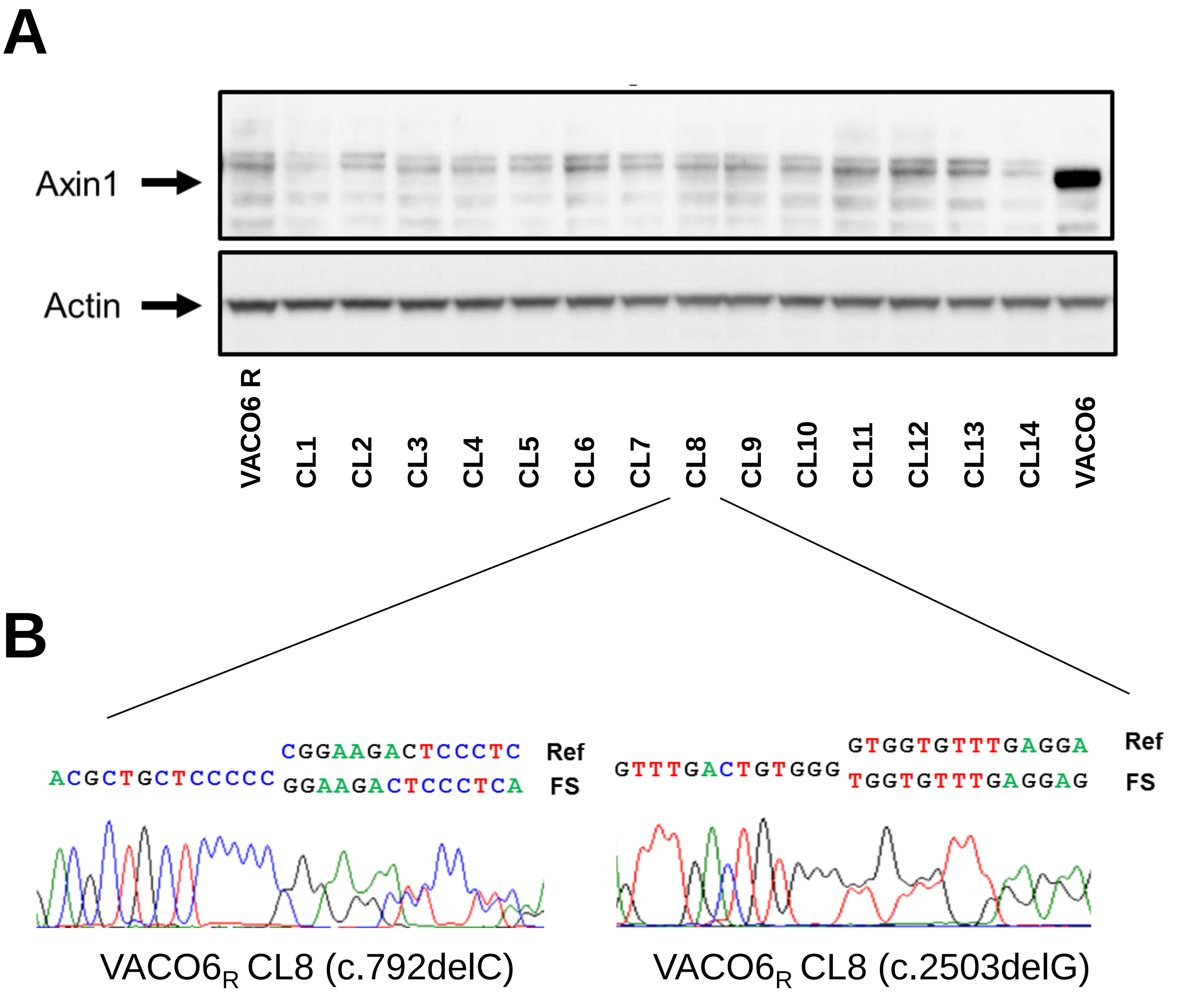

Picco et al., Appendix Figure S6. Single clone analysis of VACO6$_R$ cells.
(A) Western blot showing loss of the Axin1 protein in all 14 single cell clones derived from VACO6$_R$ population. (B) Representative chromatograms of Sanger-sequenced PCR products showing the two c.792delC and c.2503delG AXIN1 frameshift deletions in a representative clone (CL8) derived from VACO6$_R$ cells.

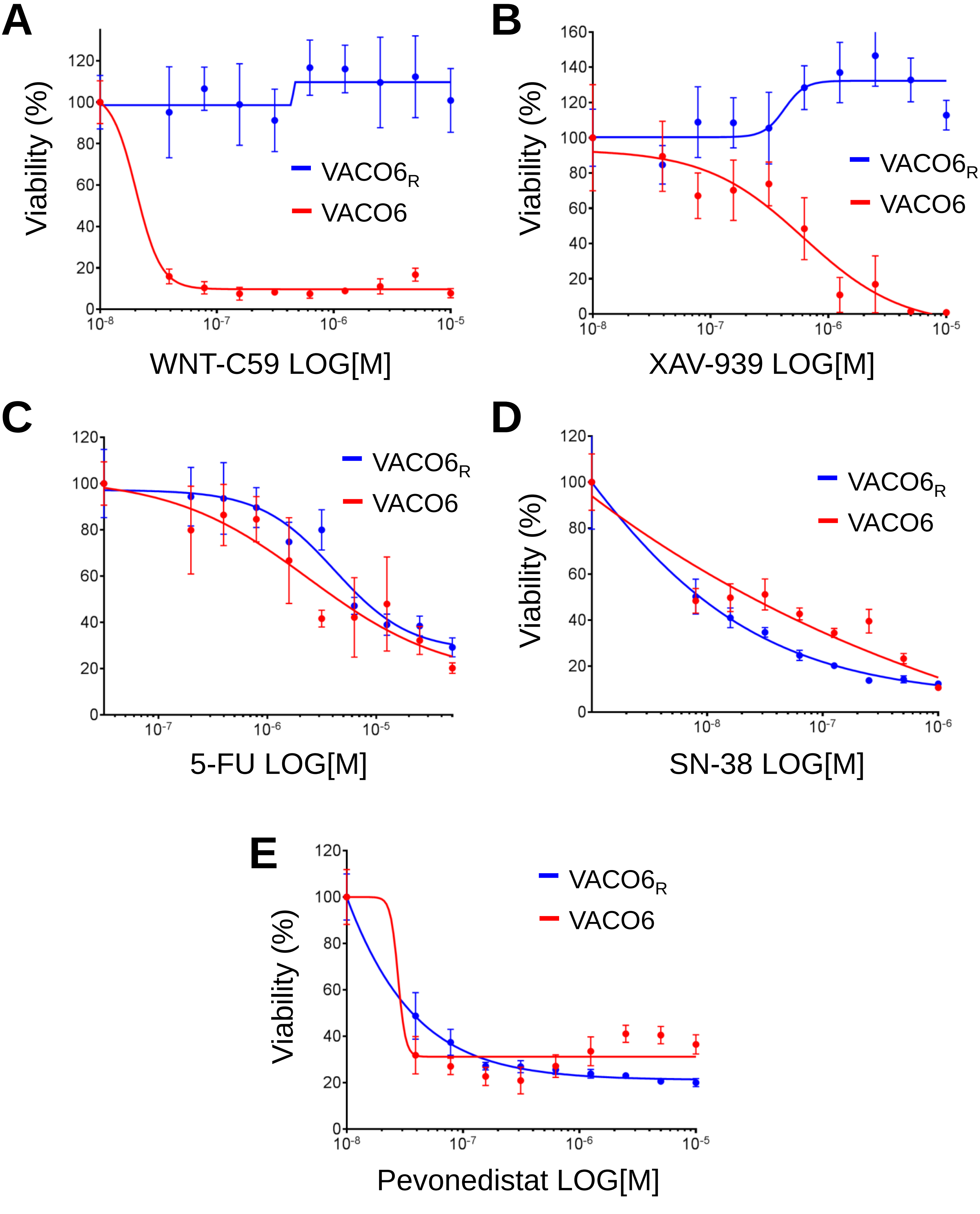

Picco et al., Appendix Figure S7. VACO6$_R$ cells are specifically resistant to WNT pathway inhibitors. ATP-based assay measuring viability of VACO6 and VACO6$_R$ cells after 7 days of treatment with WNT-C59 (A), XAV-939 (B), 5-FU (C), SN-38 (D) and Pevonedistat (E). Data are expressed as average ± s.d. of six technical replicates

Picco et al. Appendix Table S1A. RSPO2/3 fusion analysis in TCGA CRC samples. The table reports (i) the ID of CRC TGCA samples selected for the analysis (ii) the APC, KRAS and BRAF mutational status (iii) the RSPO3 mRNA levels; (iv) the CAF-signature values; (v) the level of stromal contamination, (vi) the Z-score after CAF-score correction (vii) the type of fusion trascripts identified, (viii) the tools that indentified the fusion, (ix) the number of reads supporting the fusion and (x) the type of RNA-seq reads available for the analysis.

TCGA sample ID	APC status	KRAS status	BRAF status	RSPO3 expression (Log_2 RSEM)	RSPO3 expression (Log_2 RSEM) Z-score	CAF-score (Log2)	Delta (RSPO3 - CAF-score)	Delta (RSPO3 - CAF-score) Z-score	RSPO3 fusion	Tools that identified the fusion	Number of supporting reads	RNA-seq reads type
TCGA-CA-5255				9.93	2.71	6.58	**3.35**	5.58	PTPRK(ex1)-RSPO3(ex2)	defuse, mapsplice	7	paired end
TCGA-AF-6136				10.44	3.00	7.82	**2.61**	4.95	PTPRK(ex1)-RSPO3(ex2)	chimerascan, mapsplice	5	paired end
TCGA-D5-6539				9.86	2.67	7.83	**2.03**	4.45	PTPRK(ex1)-RSPO3(ex2)	chimerascan	10	paired end
TCGA-AA-3518	WT	WT	WT	9.12	2.25	7.43	**1.69**	4.15	PTPRK(ex1)-RSPO3(ex2)	mapsplice	5	single end
TCGA-AA-3842	WT	MUT:G13D	WT	9.23	2.31	8.67	**0.56**	3.18	PTPRK(ex1)-RSPO3(ex2)	mapsplice	3	single end
TCGA-A6-2672	WT	WT	MUT:V600E	9.15	2.27	8.70	**0.45**	3.08	not detected			paired end
TCGA-DT-5265				9.87	2.67	9.54	**0.33**	2.98	PTPRK(ex1)-RSPO3(ex2)	defuse	3	paired end
TCGA-AZ-4323				9.27	2.34	9.56	**-0.29**	2.45	not detected			paired end
TCGA-AA-3695	MUT:R213*	MUT:G12D	WT	10.12	2.82	10.65	**-0.53**	2.24	not detected			single end
TCGA-F5-6812				8.90	2.13	9.86	**-0.96**	1.87	not detected			paired end
TCGA-CM-6167				9.33	2.37	10.85	**-1.52**	1.38	not detected			paired end
TCGA-A6-6651				8.83	2.09	10.55	**-1.72**	1.21	not detected			paired end
TCGA-G4-6302				8.93	2.14	10.74	**-1.81**	1.14	not detected			paired end
TCGA-EI-7004				9.02	2.19	11.19	**-2.17**	0.83	not detected			paired end

Picco et al. Appendix Table S1B. Settings for fusion transcript search in RNAseq data with Defuse, Chimerascan and Mapsplice tools.	
tool	***parameters***

defuse (version 0.6.1)	`# Bowtie parameters`
	`bowtie_threads = 1`
	`bowtie_quals = --phred33-quals`
	`max_insert_size = 500`
	
	`# Blat sequences per job`
	`num_blat_sequences = 10000`
	
	`# Minimum gene fusion range`
	`dna_concordant_length = 2000`
	
	`# Trim length for discordant reads (split reads are not trimmed)`
	`discord_read_trim = 50`
	
	`# Filtering parameters`
	`clustering_precision = 0.95`
	`span_count_threshold = 5`
	`percent_identity_threshold = 0.90`
	`split_min_anchor = 4`
	`splice_bias = 10`
	`probability_threshold = 0.50`

chimerascan (version 0.4.5)	`-p 32 --library-type fr-firststrand --multihits 50 --initial-mismatches 1 --discord-mismatches 2 --segment-length 40 --homology-mismatches 1 --anchor-min 6 --anchor-length 12 --filter-unique-frags 4.0`
mapsplice (version 2.1.8)	`--fusion-non-canonical --threads 32`

Appendix Table S2A. Point mutations detected by exome sequencing of $VACO6_R$ cells compared to VACO6 cells.

GENE ID	Cohordinates	Nucleotide change	Effect on translation	AA change	Position depth VACO6	Position depth $VACO6_R$	% mutant reads	Occurrences in Cosmic
CDK18	chr1:205498487	c.G1198A	nonsyn.	p.A400T	164	115	43	2
PNKP	chr19:50365045	c.G1282T	nonsyn.	p.A428S	333	296	38	2
AP1M1	chr19:16339599	c.C943T	nonsyn.	p.R315W	128	158	37	2
OCM2	chr7:97619395	c.A22T	nonsyn.	p.S8C	101	115	43	1
MAP4K3	chr2:39553363	c.G586T	nonsyn.	p.D196Y	128	135	7	1
SDHA	chr5:256455	c.C1915G	nonsyn.	p.L639V	320	281	4	1
ZCCHC12	chrX:117960084	c.C877T	nonsyn.	p.P293S	113	103	79	0
NXF3	chrX:102334704	c.G1147A	nonsyn.	p.E383K	51	53	66	0
COL9A3	chr20:61452558	c.C335A	nonsyn.	p.P112H	172	151	55	0
AIF1L	chr9:133995659	c.C481G	nonsyn.	p.P161A	100	95	52	0
ZNF134	chr19:58132760	c.G1273T	nonsyn.	p.G425C	115	98	51	0
ARHGAP21	chr10:24874647	c.T4571C	nonsyn.	p.L1524P	137	108	48	0
DLGAP3	chr1:35370359	c.A626T	nonsyn.	p.D209V	111	129	47	0
EIF4G1	chr3:184049311	c.C4333T	nonsyn.	p.L1445F	298	290	46	0
LCA5L	chr21:40795085	c.G654T	nonsyn.	p.Q218H	134	152	45	0
NOL8	chr9:95078363	c.T544C	nonsyn.	p.F182L	75	94	45	0
SORCS3	chr10:106401117	c.G32A	nonsyn.	p.G11D	87	77	44	0
FLRT3	chr20:14307220	c.C933A	stopgain	p.C311*	165	167	43	0
SRRD	chr22:26879962	c.G106C	nonsyn.	p.G36R	19	25	40	0
AP1M1	chr19:16339598	c.G942T	nonsyn.	p.K314N	122	146	40	0
ANKRD6	chr6:90340265	c.C1726A	nonsyn.	p.Q576K	178	186	39	0
SCFD2	chr4:54231369	c.C740T	nonsyn.	p.A247V	116	140	39	0
SEMA6B	chr19:4558147	c.C136T	nonsyn.	p.P46S	37	39	38	0
LRRC10B	chr11:61276987	c.G517T	stopgain	p.E173*	151	127	38	0
FUK	chr16:70506992	c.C1513A	nonsyn.	p.L505M	130	120	38	0
ADH6	chr4:100131372	c.G434A	nonsyn.	p.S145N	215	259	37	0
CYP46A1	chr14:100191750	c.G1199A	nonsyn.	p.R400Q	104	77	36	0
NUTM2F	chr9:97081325	c.G1693T	nonsyn.	p.V565L	118	111	36	0
SEC16B	chr1:177927999	c.G1110T	nonsyn.	p.L370F	75	93	34	0
AKAP9	chr7:91708592	c.A7145T	nonsyn.	p.D2382V	240	230	34	0
TTN	chr2:179429009	c.G81850A	nonsyn.	p.V27284I	248	256	34	0
AKAP9	chr7:91708591	c.G7144A	nonsyn.	p.D2382N	257	247	33	0
LPPR3	chr19:813427	c.G1384A	nonsyn.	p.A462T	158	101	32	0
LYPD3	chr19:43965642	c.C902A	nonsyn.	p.A301D	222	210	31	0
KIAA0430	chr16:15729770	c.C574T	nonsyn.	p.P192S	251	211	31	0
POU5F1	chr6:31138186	c.G212T	nonsyn.	p.G71V	205	200	31	0
KCNK15	chr20:43379012	c.G526A	nonsyn.	p.V176I	265	192	30	0
RASGRF1	chr15:79291149	c.G2813T	nonsyn.	p.R938M	207	207	29	0
RBM15B	chr3:51430792	c.C1962A	nonsyn.	p.S654R	131	124	25	0
AKAP3	chr12:4737115	c.T953C	nonsyn.	p.L318P	272	269	21	0
RBM15B	chr3:51430809	c.C1979T	nonsyn.	p.A660V	129	111	21	0
LMO1	chr11:8251938	c.G139A	nonsyn.	p.D47N	205	254	20	0
MRPL42	chr12:93870791	c.T132G	nonsyn.	p.N44K	117	121	18	0
SLC2A3	chr12:8075523	c.T1166C	nonsyn.	p.V389A	202	219	15	0
ABCA4	chr1:94496009	c.C4327T	nonsyn.	p.R1443C	333	341	14	0
OLFML2B	chr1:161993133	c.G88A	nonsyn.	p.E30K	70	81	12	0
NUTM2G	chr9:99700853	c.G1648T	nonsyn.	p.V550L	368	342	9	0
LRRC15	chr3:194081462	c.G329A	nonsyn.	p.R110H	178	193	9	0
ZFP64	chr20:50701323	c.G1711C	nonsyn.	p.V571L	225	204	9	0
TTN	chr2:179658207	c.A1460T	nonsyn.	p.K487M	124	149	9	0
FGG	chr4:155529781	c.T688A	nonsyn.	p.F230I	141	145	8	0
CACNA1C	chr12:2711030	c.A2924G	nonsyn.	p.Y975C	331	321	8	0
KRT81	chr12:52681013	c.G1120A	nonsyn.	p.A374T	584	512	8	0
SMG7	chr1:183495830	c.G412A	nonsyn.	p.A138T	131	143	8	0
CACNA1C	chr12:2774080	c.C4466A	nonsyn.	p.T1489K	339	323	7	0
GCNT2	chr6:10529656	c.T512C	nonsyn.	p.L171P	189	177	7	0
TRIM26	chr6:30154018	c.T1255G	nonsyn.	p.L419V	117	155	7	0
WDR35	chr2:20131104	c.G2923A	nonsyn.	p.A975T	178	171	7	0
KIRREL	chr1:158064767	c.G2131T	nonsyn.	p.A711S	131	181	7	0
ATF7	chr12:53937094	c.C284T	nonsyn.	p.A95V	273	269	6	0
ZNF726	chr19:24116410	c.G1492A	nonsyn.	p.A498T	186	203	6	0
PCDHB13	chr5:140595593	c.G1898A	nonsyn.	p.R633H	292	242	6	0
MCAT	chr22:43529240	c.C982T	stopgain	p.Q328*	269	246	5	0
MUC17	chr7:100678112	c.A3415C	nonsyn.	p.S1139R	368	355	5	0
IGFN1	chr1:201178696	c.G4675C	nonsyn.	p.G1559R	218	179	5	0
TF	chr3:133467417	c.A205G	nonsyn.	p.R69G	228	196	5	0
MUC17	chr7:100678130	c.G3433T	nonsyn.	p.A1145S	399	364	4	0
NOMO1	chr16:14969038	c.A2200C	nonsyn.	p.T734P	439	429	2	0

Appendix Table S2B. Insertions / deletions detected by exome sequencing of $VACO6_R$ cells compared to VACO6 cells.

GENE ID	Cohordinates	Insert / Del	Indel size	Effect	Position depth VACO6	Position depth $VACO6_R$	% altered reads	Occurrences in COSMIC
AXIN1	chr16:396233-396235	Del	D-1	frameshift	248	127	26	1
AXIN1	chr16:338207-338209	Del	D-1	frameshift	438	357	25	1
PCDH12	chr5:141324955-141324956	Insert	I-9	in-frame	101	60	57	17
ATXN2L	chr16:28847349-28847351	Del	D-1	frameshift	20	17	65	8
BRD7	chr16:50368677-50368680	Del	D-2	frameshift	121	148	11	7
EP400	chr12:132547093-132547094	Insert	I-9	in-frame	355	97	33	6
EP400	chr12:132547093-132547094	Insert	I-6	in-frame	355	91	29	6
OR2T2	chr1:248616704-248616712	Del	D-7	frameshift	428	370	5	5
KCNN3	chr1:154842199-154842200	Insert	I-9	in-frame	221	28	61	4
KCNN3	chr1:154842199-154842200	Insert	I-6	in-frame	221	24	54	4
NOS1	chr12:117703229-117703230	Insert	I-1	frameshift	124	116	13	4
OR8D4	chr11:123777441-123777443	Del	D-1	frameshift	182	117	9	4
IFRD1	chr7:112108038-112108040	Del	D-1	frameshift	314	297	28	3
NUMA1	chr11:71746964-71746966	Del	D-1	frameshift	139	119	8	3
GCN1	chr12:120595736-120595740	Del	D-3	in-frame	231	198	5	3
WRN	chr8:30945376-30945380	Del	D-3	in-frame	304	283	4	3
TMEM229A	chr7:123672456-123672460	Del	D-3	in-frame	117	88	65	2
KCNN3	chr1:154842199-154842200	Insert	I-9	in-frame	221	28	61	2
KCNN3	chr1:154842199-154842200	Insert	I-6	in-frame	221	24	54	2
HPS1	chr10:100186986-100186987	Insert	I-1	frameshift	159	164	30	2
KCNN3	chr1:154842199-154842200	Insert	I-9	in-frame	221	28	61	1
KCNN3	chr1:154842199-154842200	Insert	I-6	in-frame	221	24	54	1
CLDN6	chr16:3065485-3065487	Del	D-1	frameshift	76	42	38	1
MMP10	chr11:102650394-102650395	Insert	I-1	frameshift	208	183	34	1
EP400	chr12:132547093-132547094	Insert	I-9	in-frame	355	97	33	1
EP400	chr12:132547093-132547094	Insert	I-6	in-frame	355	91	29	1
PRRC2A	chr6:31602640-31602642	Del	D-1	frameshift	301	244	24	1
ZNF717	chr3:75786894-75786896	Del	D-1	frameshift	879	118	24	1
ZNF717	chr3:75786555-75786556	Insert	I-2	frameshift	737	107	19	1
UNC93B1	chr11:67771217-67771221	Del	D-3	in-frame	231	152	7	1
BHLHE22	chr8:65494020-65494024	Del	D-3	in-frame	221	179	6	1
RPL14	chr3:40503520-40503521	Insert	I-3	in-frame	143	43	74	--
RPL14	chr3:40503520-40503521	Insert	I-6	in-frame	143	39	72	--
ATG3	chr3:112253058-112253059	Insert	I-1	frameshift	82	30	53	--
TRIL	chr7:28997596-28997597	Insert	I-1	frameshift	143	99	46	--
RAPGEF6	chr5:130764796-130764801	Del	D-4	frameshift	157	149	46	--
EOMES	chr3:27763427-27763428	Insert	I-6	in-frame	79	43	37	--
WI2-2373I1.2	chr7:331127-331131	Del	D-3	in-frame	33	41	37	--
ARV1	chr1:231131566-231131569	Del	D-2	frameshift	151	144	35	--
KIR2DL4	chr19:55324674-55324675	Insert	I-1	frameshift	253	157	35	--
BCAR1	chr16:75269741-75269743	Del	D-1	frameshift	65	54	33	--
MAML3	chr4:140811063-140811079	Del	D-15	in-frame	190	55	33	--
CWC22	chr2:180810054-180810057	Del	D-2	frameshift	122	105	30	--
SEC14L2	chr22:30805433-30805435	Del	D-1	frameshift	178	144	28	--
ARID1B	chr6:157099426-157099427	Insert	I-6	in-frame	125	105	28	--
NRP2	chr2:206562375-206562377	Del	D-1	frameshift	263	211	27	--
GALNT5	chr2:158167772-158167774	Del	D-1	frameshift	80	87	24	--
CCDC159	chr19:11461508-11461510	Del	D-1	frameshift	103	105	20	--
ZNF880	chr19:52887149-52887247	Del	D-97	frameshift	110	54	19	--
HLA-A	chr6:29912028-29912031	Del	D-2	frameshift	340	190	16	--
PMS1	chr2:190670378-190670380	Del	D-1	frameshift	219	182	12	--
ANKRD36C	chr2:96592972-96593062	Del	D-89	frameshift	285	161	11	--
MUC5B	chr11:1267447-1271222	Del	D-3774	in-frame	353	132	11	--
PRKRA	chr2:179301046-179307993	Del	D-6946	frameshift	16	175	9	--
SLC10A5	chr8:82606649-82606650	Insert	I-1	frameshift	128	138	8	--
MAPKBP1	chr15:42092079-42092081	Del	D-1	frameshift	130	126	8	--
MUC5B	chr11:1267611-1271470	Del	D-3858	in-frame	346	213	8	--
TLR4	chr9:120476083-120476084	Insert	I-1	frameshift	209	185	7	--
MUC5B	chr11:1267306-1271078	Del	D-3771	in-frame	352	187	6	--
POTED	chr21:14982606-14982607	Insert	I-111	in-frame	336	197	6	--
MUC12	chr7:100637861-100642533	Del	D-4671	in-frame	891	338	5	--
AXIN1	chr16:354362-354364	Del	D-1	frameshift	335	285	4	--
HRNR	chr1:152188231-152191052	Del	D-2820	in-frame	1279	1261	2	--
MUC12	chr7:100642276-100645526	Del	D-3249	in-frame	1106	848	2	--
MUC12	chr7:100643201-100646451	Del	D-3249	in-frame	1092	818	2	--
MUC12	chr7:100642062-100645312	Del	D-3249	in-frame	1198	1364	2	--